DARK CURRENT AND PHOTOCURRENT IN RETINAL RODS

W. A. HAGINS, R. D. PENN, *and* S. YOSHIKAMI

From the National Institute of Arthritis and Metabolic Diseases, National Institutes of Health, Bethesda, Maryland 20014

ABSTRACT The interstitial voltages, currents, and resistances of the receptor layer of the isolated rat retina have been investigated with arrays of micropipette electrodes inserted under direct visual observation by infrared microscopy. In darkness a steady current flows inward through the plasma membrane of the rod outer segments. It is balanced by equal outward current distributed along the remainder of each rod. Flashes of light produce a photocurrent which transiently reduces the dark current with a waveform resembling the PIII and a-wave components of the electroretinogram. The photocurrent is produced by a local action of light within 12 μm of its point of absorption in the outer segments. The quantum current gain of the photocurrent is greater than 10^6. The electrical space constant of rat rods is greater than 25 μm, so that the electrical effects of the photocurrent are large enough at the rod synapses to permit single absorbed photons to be detected by the visual system. The photocurrent is apparently the primary sensory consequence of light absorption by rhodopsin.

INTRODUCTION

The photoreceptor cells of the vertebrate retina have long been thought to produce electric currents which contribute one or more components to the electroretinogram (ERG) (see review by Granit, 1963) and which might explain the recent observation that rods and cones hyperpolarize when illuminated. The origin and spatial distribution of these currents are of interest because of their possible function in transmitting signals from the outer segments, where photons are absorbed, to the receptor synapses with the distal neurons of the visual system. Although analyzing the electrical activity of vertebrate rods and cones would seem simple, it has not proved to be. Largely this is because it is difficult to locate microelectrodes precisely in the photoreceptor layer without using light microscopy which the great light sensitivity of the retina forbids. This paper reports an analysis of the currents, voltages, and resistances in the interstitial spaces of the receptor layer of the rat retina by a method using infrared microscopy to aid in electrode placement. Preliminary accounts have appeared previously (Penn and Hagins, 1969 *a*, *b*). The second paper of this series examines the kinetics of the rod photocurrent in more detail.[1]

[1] Penn, R. D., and W. A. Hagins. Manuscript in preparation.

SYMBOLS

x, y, z	distances measured from an origin at the center of the face of a slice containing the rod tips radially into the slice (x), horizontally along the longest dimension of the slice (y), and vertically in the direction Z of propagation of stimulus beams. (μm)
r_{xx}, r_{yy}, r_{zz}	resistivities of slice for currents flowing in the X, Y, Z directions. (ohm cm)
g_{xx}, g_{yy}, g_{zz}	conductivities (reciprocals of above resistivities). (mho cm^{-1})
a	interelectrode spacing. (μm)
V	potential at a point in interstitial space. (volts)
$V_m(x)$	potential difference across the plasma membrane of a rod at distance x from tip of its outer segment. (volts)
i_x, i_y, i_z	components of interstitial currents in retina parallel to coordinate axes. (amp cm^{-2})
i_{xx}, i_{yy}, i_{zz}	components of divergence of interstitial current parallel to coordinate axes. (amp cm^{-3})
$i_m(x, y, z)$	divergence of interstitial current at point x, y, z. (amp cm^{-3})
$\bar{r}_{xx}(x)$	average of r_{xx} over interval. (x-a, x)
ρ	resistivity of physiological solution. (ohm cm)
$R_C(x)$	radial resistance of cytoplasm of a single rod. (ohm cm^{-1})
$R_E(x)$	radial resistance of interstitial space surrounding a single rod in retinal mosaic. (ohm cm^{-1})
L	total length of a rod. (cm)
$G(x)$	conductance of rod plasma membrane. (mho cm^{-1})
G_m	conductance of rod plasma membrane per unit area. (mho cm^{-2})
$\phi(x)$	density of source current generated in rod plasma membrane. (amp cm^{-1})
$J(x)$	net current through plasma membrane. (amp cm^{-1})
$\beta(x)$	$\equiv R_E(x)/(R_E[x] + R_C[x])$.

THEORETICAL

The receptor layer of the vertebrate retina is a closely packed uniform mosaic of elongated cells with axes normal to the retinal surfaces. Although the cells constitute the bulk of the tissue, the conductivity of interstitial fluid is likely to be very high compared to that of typical cell membranes. Thus, it is reasonable to represent the interstitial space as a continuous conducting medium which is made inhomogenous and anisotropic by the resistance of the cell membranes. Where there is a net transmembrane current, there will appear to be a current source or sink in the medium. In such a medium, the potential V is related to the distribution i_m of sources and sinks by the divergence theorem.

$$\nabla \cdot \boldsymbol{g} \nabla V = -i_m \qquad (1)$$

where ∇ is the vector differential operator and $\boldsymbol{g}$ is the conductivity tensor of the tissue (e.g. see Jeans, 1951, p. 345). If the coordinate axes are chosen parallel to the principal axes of tissue conductivity (Carslaw and Jaeger, 1959, pp. 38–49) (which for the photoreceptor layer would be a rectangular coordinate system parallel and perpendicular, respectively, to the main axis of tissue symmetry, the lengths of the

photoreceptor cells), the conductivity is resolved into three perpendicular components, g_{xx}, g_{yy} and g_{zz}. Equation 1 then becomes

$$-i_m(x, y, z) = \frac{\partial}{\partial x}\left(g_{xx}\frac{\partial V}{\partial x}\right) + \frac{\partial}{\partial y}\left(g_{yy}\frac{\partial V}{\partial y}\right) + \frac{\partial}{\partial z}\left(g_{zz}\frac{\partial V}{\partial z}\right) \qquad (2\,a)$$

or

$$-i_m = i_{xx} + i_{yy} + i_{zz}. \qquad (2\,b)$$

At the same time, Ohm's law requires that

$$-i_x = g_{xx}\frac{\partial V}{\partial x}, \qquad -i_y = g_{yy}\frac{\partial V}{\partial y}, \qquad -i_z = g_{zz}\frac{\partial V}{\partial z}, \qquad (3)$$

where i_x, i_y, and i_z are the components of current in the interstitial spaces parallel (i_x) and perpendicular (i_y and i_z) to the rod axes. (See Fig. 1.)

In the experiments described in this paper, the spatial distribution of membrane current of rods is estimated by means of equation 2. The voltage gradients are measured with arrays of microelectrodes placed at known positions in the interstitial spaces of the photoreceptor layer. The conductivities are, in turn, estimated with the same arrays of electrodes together with currents applied to the retina from large external electrodes. In calculating i_m, allowance is made for the finite spacing of the recording electrodes (Appendix I).

For this method to be valid, three general conditions must hold. (*a*) *The uniformity condition.* While the interstitial space of tissue may be inhomogeneous, its passive electrical properties must be uniform in a certain sense and must vary slowly on the scale of spatial resolution at which the pattern of sources and sinks is to be measured. For example, if two electrodes are placed at equal radial depths, they should record equal voltages relative to an electrode at the tissue surface when a uniform radial current is applied from external electrodes. Thus, the area of retina studied must be flat and free of holes, injured areas, blind pockets with highly resistive boundaries, etc. (*b*) *The constant impedance condition.* The interstitial conductivity g must be independent of time and interstitial current. That is, current flowing through the capacitance of the cell membranes or through voltage-sensitive conductances must be negligible in relation to that flowing in the ohmic part of the intracellular spaces. (*c*) *The objectivity condition.* The presence of the recording electrodes must not distort the interstitial conductance or voltage field appreciably.

It is difficult to formulate these conditions quantitatively and to show by experiment that they hold exactly. Nevertheless, two steps were taken to avoid complications due to their possible failure. First, the rat retina was used, because its photoreceptor layer is uniform and contains a very fine-grained mosaic of small rod cells with essentially no cones (Walls, 1942). Second, simple checks which would detect

gross violation of the underlying assumptions were applied. These are described in the Results.

METHODS

Albino rats were dark-adapted for 10 min and killed by intraperitoneal injection of pentobarbital (50 mg/kg). An eye was excised in dim red light and its retina dissected free in a bath of oxygenated physiological solution. An infrared light source and a binocular dissecting microscope fitted with infrared image converters were used to permit the retina to remain dark-adapted during preparation. A segment of retina extending from optic nerve to far periphery was placed receptor-side-up on a piece of Millipore type HA membrane filter (Millipore Filter Corp., Bedford, Mass.). The filter was then placed on a blotter and the excess fluid was removed. The retina was drawn down against the filter by capillarity so that the two subsequently adhered tenaciously. The filter was immediately replaced in the bath and sliced into strips of width 50–300 μm by a stainless steel razor blade fixed in a micromanipulator. A filter strip with its attached slice of retina was transferred to a shallow chamber (Fig. 1) on the stage of an inverted microscope. The chamber was held at 33–35°C by conduction from the heated stage. A stream of oxygenated physiological solution (Table I) was directed past the retinal slice at a rate of about 0.05 ml per min by a pair of pipettes. The filter strip and retinal slice were fastened by thin glass wedges held down with silicone stopcock grease. The slice was oriented so that the axes of the rod outer segments were parallel to the microscope stage, thus permitting all of the retinal layers to be viewed in profile by bright-field infrared microscopy. Light stimuli were also focused on the slice by the microscope's condensing optics. Image converters and a camera attached to the microscope allowed the position of retina, electrodes, and stimuli to be recorded as the experiment proceeded.

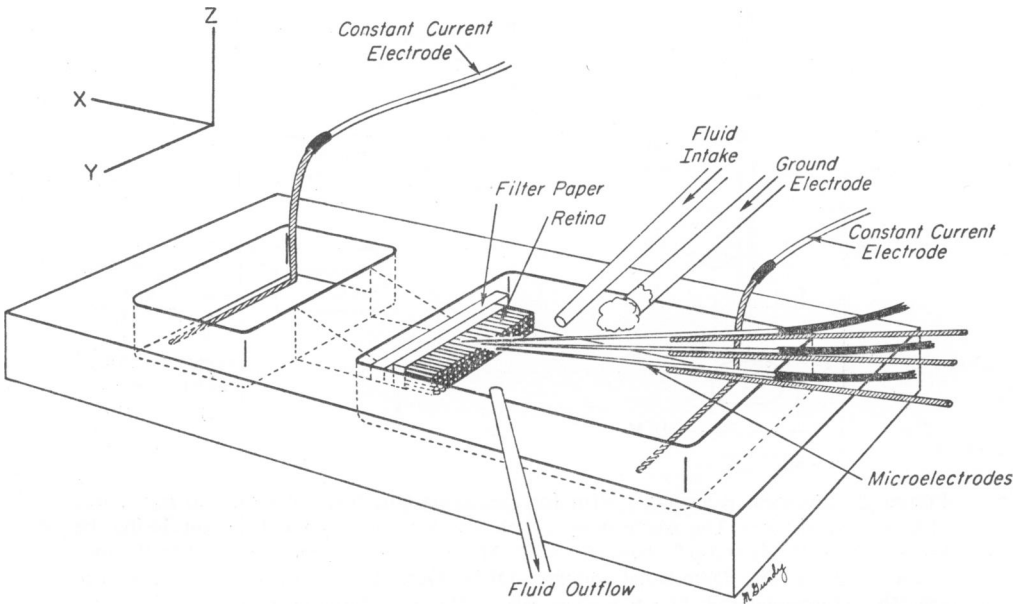

FIGURE 1. Schematic view of perfusion chamber used for recording from living retinal slices.

The retinal slice was covered at its ends and its upper and lower surfaces by thin glass barriers so that current applied from the constant current electrodes (Fig. 1) was forced to flow radially through the tissue from the large bath to the small one.

TABLE I
COMPOSITION OF PHYSIOLOGICAL SOLUTIONS

	Ringer I	Ringer II
	mM	*mM*
Na^+	140	137
K^+	3.5	2.7
Ca^{++}	0.18	1.36
Mg^{++}	0.18	0.5
Cl^-	147	145
$H_2PO_4^- + HPO_4^-$	12	0.73
Tris	—	10
Glucose	11	11
pH at 37°C	7.7	7.13

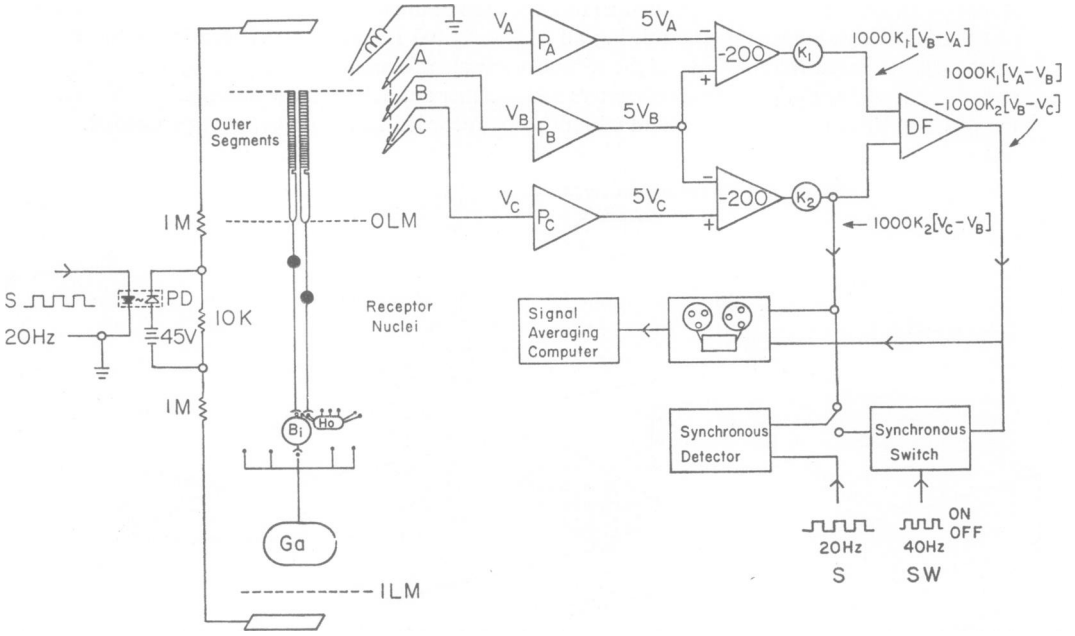

FIGURE 2 Electrical recording system for measuring currents, voltages, and resistances of living retinal slices. The synchronous switch SW was phased so as to be on during the last half of each on-and-off phase of the 20 Hz square-wave generator S. PD: Photon-coupled isolator. DF: Differential amplifier. OLM: Outer limiting membrane. Bi: Bipolar cell. Ho: Horizontal cell. Ga: Ganglion cell. ILM: Inner limiting membrane. A, B, C: Micropipette electrodes filled with 0.15 M NaCl + 0.01 M Tris (pH 7.4) and with tip diameters of ~1–2 μm and resistances of ~5–10 MΩ.

A large wick electrode near the slice grounded the large chamber. An array of one to three glass pipette electrodes was held in position in the tissue by a micromanipulator fitted with a linear displacement transducer, which displayed radial movements of the array as the horizontal displacement on an X-Y plotter with a resolution of ± 1 μm. The electrode tips were usually 1–2 μm in diameter and thus were large enough to be seen while inserted in slices thinner than 100 μm. However, the displacement transducer was relied upon to give exact electrode positions. The retina was simply observed through the microscope to assure that no appreciable distortion of tissue or pipettes occurred during penetration. The electrodes were filled with 0.15 M NaCl solution containing 10 mM Tris buffer (pH 7.4).

The electrical apparatus is shown in Fig. 2. Each microelectrode A, B, and C was connected to a DC coupled capacitance-compensated preamplifier P with a first-order risetime of 500 μsec to an input voltage step, an input bias current of *circa* 0.2 pa and a gain of +5.00. Two secondary DC amplifiers with adjustable attenuators K_1 and K_2 produced outputs proportional to $V_A - V_B$ and $V_B - V_C$, respectively. These voltage differences were then amplified, averaged, and recorded. Transretinal currents were injected through the slice from an electrically isolated pulse generator switched on and off via a light-emitting diode coupled to a photoconductive diode. The current pulses had rise and fall times of less than 50 μsec and were equivalent in amplitude to the flow of 800 μa cm^{-2} of retina or less. Leakage from the current pulse generator was less than 0.1 μa cm^{-2} with the diode switched off.

Light stimuli were obtained from xenon flashtubes with flash durations of about 2 μsec. Interference filters and calibrated neutral density filters spectrally shaped and attenuated the flashes. Absolute flash exposures (hν cm^{-2}) at the retinas were measured to $\sim$ 10% accuracy with calibrated silicon photovoltaic detectors. In most cases a spectral band of 15 nm half-width centered at 560 nm was used. This wavelength region is weakly absorbed by rhodopsin, so that the flashes penetrated evenly through a 200 μm layer of rods without being unduly attenuated by the outer segments closest to the source.

RESULTS

The Structure of Rods and the Impedance of the Receptor Layer

Since the shape and packing of rods should affect the passive electrical properties of the interstitial space as well as the distribution of current sources in it, the structure of the receptor layer was first studied. Dark-adapted retinas dissected in Ringer I were fixed in 4% glutaraldehyde in Ringer I buffered to pH 7.4, and embedded in Maraglas. Fig. 3 shows a phase contrast light micrograph (Fig. 3 A) of a typical section and electron micrographs of cross-sections of the receptor layer at the inner-outer segment junctions (Fig. 3 B) and in the outer nuclear layer (Fig. 3 C). Measurements of the dimensions of the various parts of the rods, corrected for 15% shrinkage during fixing and embedding are given in Table II. Both width and length of the outer segments were somewhat greater than the values given by Sidman (1957), but our light and electron microscopical measurements were in close agreement. Although the mitochondria were slightly swollen and the plasma membranes were irregular, such retinas gave stable and reproducible electrical responses for many hours.

It is clear that the rods and glial (Müller) cells are closely packed in the outer nuclear layer, but the interstitial spaces are much larger among the outer and inner

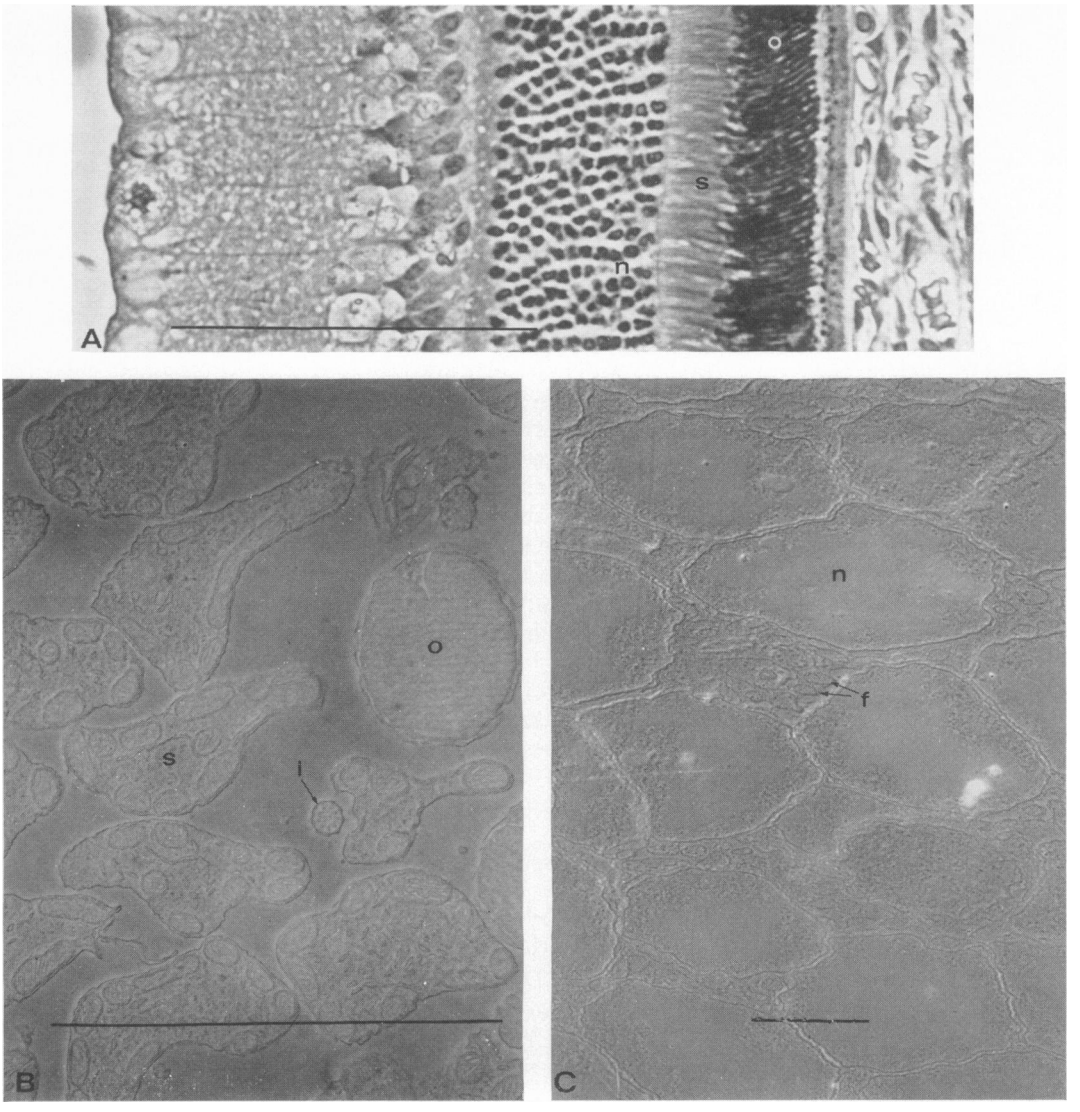

FIGURE 3 Elements of the receptor layer of the rat retina. Glutaraldehyde-osmium fixation. Epoxy embedding. Dimensions corrected for 15% shrinkage of tissue during preparation.

(A) Phase photomicrograph of a radial section through the rat retina. Calibration: 100 μm.

(B) Electron micrograph of a tangential section through the inner-outer segment junction. Sections of outer segments (o), rod necks (i), and inner segments (s) are shown. Calibration: 5 μm.

(C) Electron micrograph of a tangential section through the outer nuclear layer. Rod nuclei (n) and the thin rod fibers (f) of rods whose nuclei lie above and below the plane of the section are visible. The interstices between rod fibers and nuclei are largely filled with cytoplasm of glial (Müller) cells. Calibration: 5 μm.

TABLE II

DIMENSIONS OF 85 RAT RODS

Corrected for 15% shrinkage during embedding

	Length	Diameter	Notes
	$\mu m \pm SE$	$\mu m \pm SE$	
Outer segment	24 ± 2	1.7 ± 0.1	*
Neck	2.0 ± 0.2	0.41 ± 0.04	
Inner segment	18 ± 1.5	1.8 ± 0.2	‡
Nucleus	6.3 ± 0.3	6.3 ± 0.3	§
Rod fiber	47 ± 4	0.43 ± 0.06	‖

Total thickness of receptor layer 98 ± 4 μm (40 measurements on 6 retinas). Density of mosaic 3.1 ± 0.3 × 10^7 receptors cm^{-2} (4 measurements on 4 retinas).

* Living rods in slices observed by infrared phase microscopy gave similar figures.

‡ Diameter calculated as mean of two perpendicular measurements.

§ Considered as spheres. In some preparations they were slightly ellipsoidal.

‖ Diameters proximal and distal to nucleus are similar.

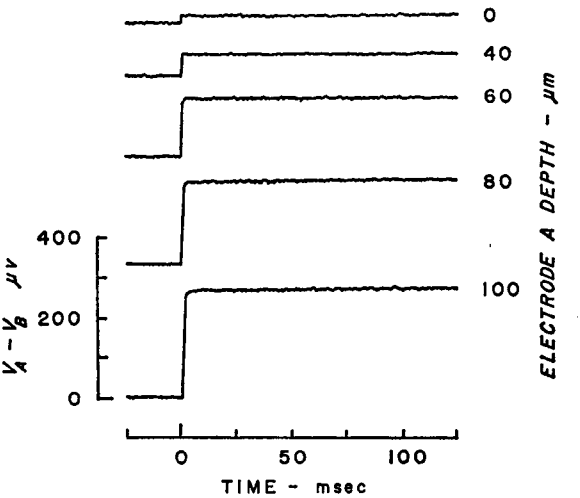

FIGURE 4 Radial voltage gradients induced in a retinal slice by radial pulses of constant current. Electrode spacing, 40 μm, with electrode A deeper than electrode B. Applied current density ~150 μa cm^{-2}. 128 pulses averaged at each electrode position.

segments. Thus, it is understandable that the interstitial resistance of the retina varies markedly with depth. This is shown in Fig. 4. A pair (A, B) of micropipettes with tips spaced 40 μm apart in a radial line was thrust radially into a slice from its choroidal surface. Square pulses of current were passed through the slice and the voltage differences ($V_A - V_B$) induced between the two electrodes were recorded at successive positions of the electrode pair. The striking increase in interstitial re-

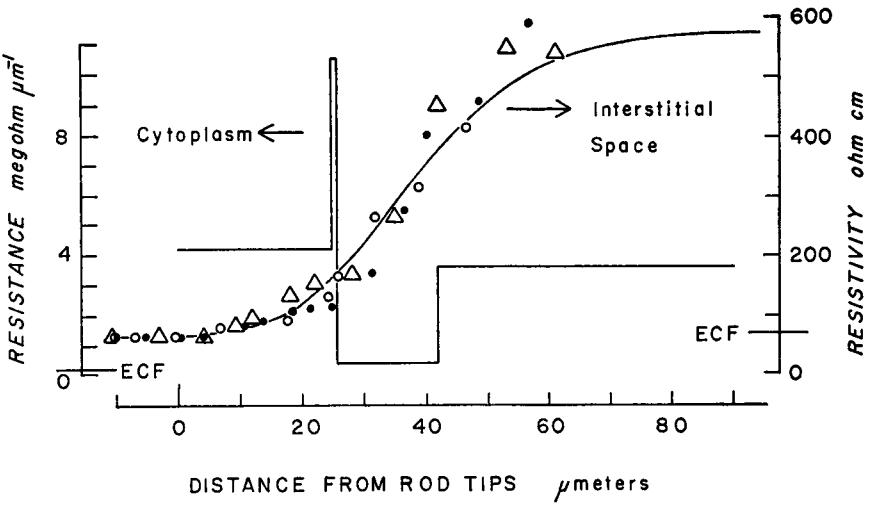

FIGURE 5 Radial interstitial and cytoplasmic resistance of rod cell layer. Extracellular fluid (ECF): Resistance of interstitial fluid.
Points: Radial interstitial resistivity of three slices for applied current pulses of ~400 μa cm^{-2}. Measuring electrode spacing, 10 μm. Read on right-hand scale.
Smooth Curve: Interpolation formula for interstitial resistance used in computing electrical constants of a model rod.
Angular Curve: Axial resistance of cytoplasm for a single rod calculated on assumptions stated in text. Read on left-hand scale. High conductivity of rod nucleus averaged over thickness of outer nuclear layer.

sistance as the electrodes moved into the outer nuclear layer was not accompanied by the appearance of any slow capacitative transients. At all depths the risetimes of the voltages were less than the 500 μsec duration of the electrical transient arising from the finite common mode rejection of the recording amplifiers. Thus, it seemed justifiable to assume that the *constant impedance condition* applied for currents flowing radially in the receptor layer.

A more detailed plot of interstitial resistance vs. depth in the receptor layer for three different slices is shown in Fig. 5. In each case the electrode spacing was 10 μm and the applied current was about 400 μa cm^{-2}, but the resistances varied by less than 2% when the current ranged between $\pm$800 μa cm^{-2}. The smooth curve is plotted from an interpolation formula which represented the interstitial resistance of the receptor layer in subsequent calculations of current flow in the rod membranes. Also shown in the figure is the internal longitudinal resistivity of a single rod calculated on the following assumptions. (*a*) The bulk conductivity of the cytoplasm is one-half that of the interstitial fluid. This approximation is based on similar ratios of interstitial to cytoplasmic conductivities in other cells (Schanne, 1969). (*b*) The internal longitudinal conductance of rods for radially flowing current is proportional to the internal cross-sectional area unobstructed by disks in the outer segments (10% of the total area) and by mitochondria in the inner segments (90% of

the total area). No great accuracy can be claimed for the calculated longitudinal conductance of the outer segments, but the conclusions to be reached are not strongly affected by four-fold errors in the values chosen.

Voltages in the Receptor Layer

Elementary properties of the active electrical responses of the rod layer will now be considered. To orient the reader, the electroretinograms of a living rat eye and of an isolated retina attached to a Millipore filter in Ringer I are shown in Figs. 6 *a* and *b*. In both there is a prominent initial upward a-wave in which the choroidal (outer) surface of the retina becomes relatively more positive with respect to the vitreal (inner) surface. A large downward b-wave follows. In Ringer II and b-wave usually disappears completely and irreversibly in 5 min to leave a relatively simple positive wave (Fig. 6 *e*) originally termed PIII by Granit (1963). When the retina is then sliced into parallel strips by radial cuts spaced at 200 μm intervals, the light-induced voltage wave across the assembly of slices becomes smaller both in Ringer II (Fig. 6 *f*), and in Ringer I (Fig. 6 *c*). The light-induced voltage gradient across the rod layer of a slice in Ringer I resembles the transretinal ERG in Ringer II. Fig. 6 *d* shows

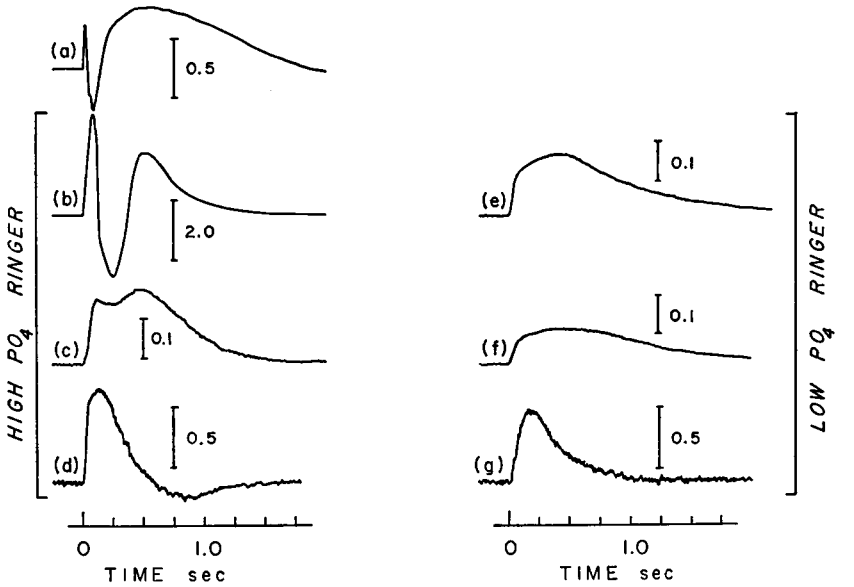

FIGURE 6 Transretinal and transreceptor voltage waveforms produced by 1 μsec light flashes. Stimuli: $\sim 10^{10}$ hν cm^{-2} (560 $\pm$ 15 nm).
(*a*) Electroretinogram of live rat at 37°C. Recorded with corneal wick electrode.
(*b*) Transretinal voltage of isolated retina in Ringer I (high PO_4). 34°C.
(*c*) Preparation of (*b*) sliced into 200 μm wide strips by radial cuts.
(*d*) Light induced voltage between electrode at rod tips and one inserted radially into slice to level of rod synapses (*circa* 100 μm deep).
(*e*), (*f*), (*g*) Preparations corresponding to (*b*), (*c*), (*d*) but in Ringer II (low PO_4). 34°C.

the voltage difference between a pipette placed at the rod tips and one in the rod-bipolar synaptic region about 100 μm deeper. Although the waveform is almost monophasic, its upward phase usually consists of at least two parts with different slopes, and there is also a late small negative wave. In Ringer II the transretinal voltage becomes a still simpler waveform (Fig. 6 *g*) which rises sigmoidally, reaches a maximum, and returns exponentially to zero. There are no negative phases and no sudden changes in slope as there are in the "PIII" response of Fig. 6 *c*. Nevertheless, the responses are quite stable and reproducible, lasting 4–6 hr with little change in amplitude or shape.

Flashes less intense than 2×10^8 hν cm^{-2} (560 nm) produce responses too small to measure accurately. At energies between 10^9 and $\sim 10^{11}$ hν cm^{-2} the responses are of constant shape with amplitudes directly proportional to light exposure. At higher energies the responses saturate in amplitude and widen. The peak amplitude ΔV_L vs. flash energy E relation[1] is of the form

$$\Delta V_L = \text{const} \times \frac{E}{E + E_1}, \tag{4}$$

where E_1 is the energy required to give a photovoltage of half-maximal amplitude. In the experiments which follow, preparations like that of Fig. 6 *g* were used, and our analysis thus applies to only one of several components in the PIII response of the rat retina.

Apart from its photovoltage, the most conspicuous electrical property of the rod layer is its steady voltage gradient in darkness. In Fig. 7 *a* plots of voltage difference between a pipette fixed at the rod tips and a moving pipette inserted into the rod layer vs. electrode depth are shown. In each of the three experiments, the penetrating electrode became progressively more positive as it approached the rod synapses. Simultaneously, the photovoltages produced by the light flashes (delivered at marks S) increased in size. In general, the dark voltage gradient and the photovoltage amplitude increased and decreased together as the electrode was inserted and withdrawn. The peak amplitude of the photovoltage never exceeded about 50% of the dark voltage gradient even with the brightest flashes. The smoothness with which the dark voltage varied with electrode depth is especially well shown in Fig. 7 *b*. *X-Y* plots of two successive insertions and withdrawals of the pipette in a slice are traced. Since there were no large discontinuities in the traces and since repeated electrode insertions gave similar results, it was assumed that the uniformity condition applied and that the electrodes did insignificant damage to the slice.

The dark voltage gradient was always found in live retinas in Ringers I and II. Changing the composition of the electrolyte in the pipettes from 0.15 to 0.3 M NaCl did not affect it, nor did the addition of ± 10 pa of input current to the preamplifier. Thus, the voltage gradient could not be attributed to the diffusion potentials often observed at liquid junctions (Overbeek, 1953) or to changes in tip resistance. When

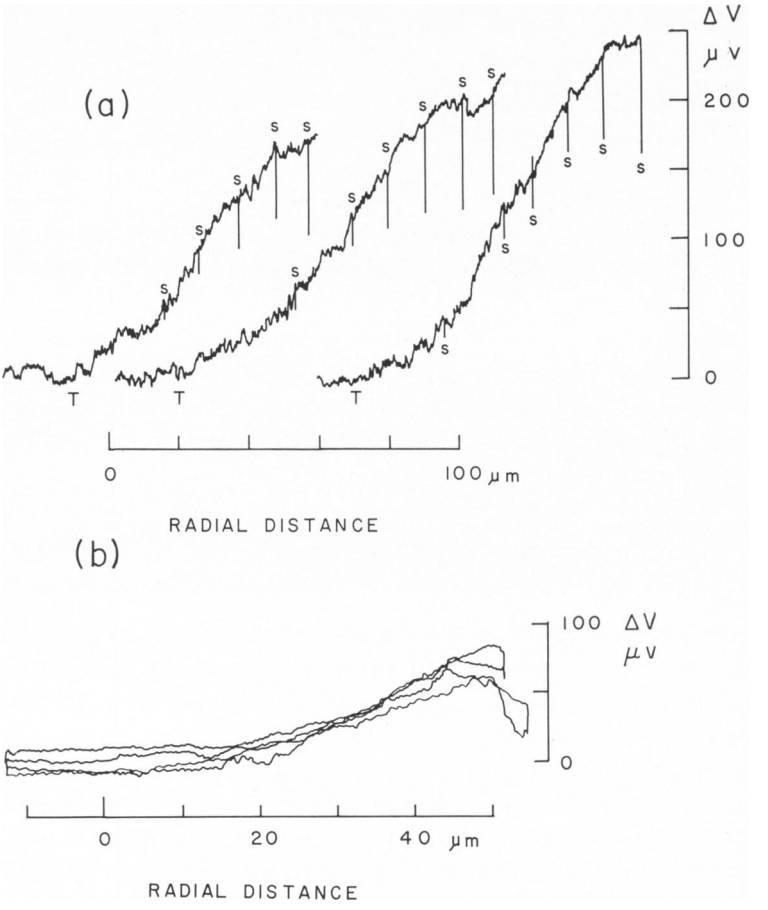

FIGURE 7 Interstitial voltage vs. radial depth in the receptor layer of a slice. Voltage differences between a pipette fixed at the tips of the outer segments and one thrust radially into the rod layer. Ringer II. 34°C.

(*a*) Records of electrode withdrawals from three different slices. 1 μsec flashes of energy $\sim 1 \times 10^{11}$ $h\nu$ cm^{-2} delivered at marks S, producing photovoltages showing as vertical lines. Moving electrode passed tips of outer segments at T.

(*b*) Two cycles of insertion and withdrawal of penetrating electrode from a single slice. The tracings reproduce within ±20%. Abscissa: Radial distance from rod tips to moving electrode.

the bath was made 10 mM in KCN, however, the dark voltage gradient disappeared within 2 min. Thus, its presence apparently depends upon oxidative metabolism (Penn and Hagins, 1969 *b*).

Origin of the Photovoltage in the Illuminated Zone of a Slice

When a small group of rods in a slice is illuminated, a small photovoltage with a waveform like that described can be detected with microelectrodes, but only if they

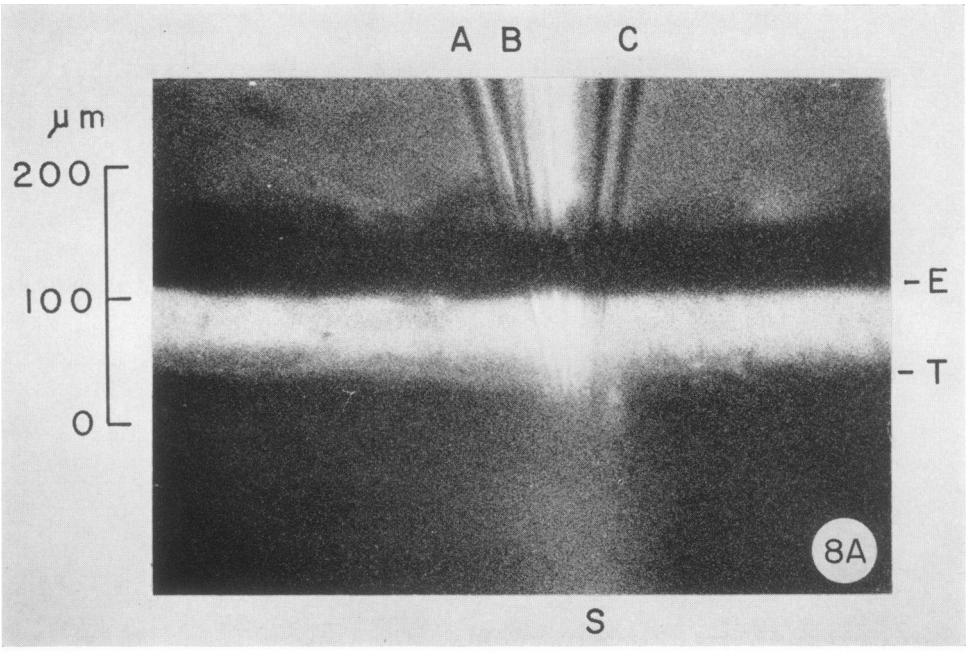
A B C
μm
200
100
0
-E
-T
8A
S

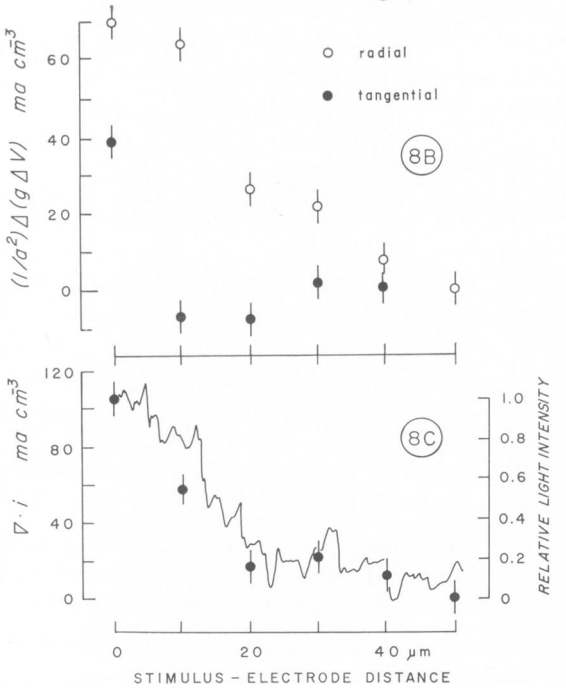
radial
tangential
8B
8C
60
40
20
0
120
80
40
0
1.0
0.8
0.6
0.4
0.2
0
0
20
40 μm
STIMULUS - ELECTRODE DISTANCE
RELATIVE LIGHT INTENSITY

are inserted into the rod layer near the light. This suggests that the photovoltage is a local response of the illuminated cells. As a more quantitative test of this notion, the spatial pattern of interstitial current at a depth of 40 μm in the receptor layer in a locally illuminated slice was compared with the distribution of the incident light. A 200 μm thick slice was illuminated with flashes which were directed downward through the receptors as a beam with a slit shaped cross-section. The long axis of the slit was parallel to the rod axes and the direction of propagation of the light was perpendicular to them and to the long axis of the slice. The geometrical width of the beam was about 12 μm at its focus about halfway through the receptor layer, but the light diverged above and below focus because the numerical aperture of the condensing optics was 0.20 and because of scattering. Figure 8 A shows a photograph of the beam end-on as it emerged from the slice slightly diffused. The beam's long axis was parallel to the right and left margins of the page. Its lower end is indicated by S. Above the ends of the outer segments the beam missed the retina but passed through a cluster of three microelectrodes.

The membrane current set up in the rods by the light at a depth of 40 μm in the slice was measured with an array of three microelectrodes, A, B, and C. Since the same procedure was used repeatedly in subsequent sections of this paper, a detailed description will be given. The three electrodes were first placed in a radial line outside the slice with their tips about 35 μm (A), 20 μm (B), and 5 μm (C) from the ends of the rods. The radial interelectrode spacing a was thus 15 μm. Radial current square waves of frequency 20 Hz and intensity I amp cm^{-2} of retina were passed through the retina and its adjacent bathing fluid. The attenuators K_1 and K_2 (Fig. 2) were set to 1.0 and the interelectrode voltage differences $\Delta V(x)$ $(= V_A[x] - V_B[x + a])$ and $\Delta V(x + a)$ $(= V_B[x + a] - V_B[x + 2a])$ produced by the current were measured. By adjusting the electrode spacings slightly, $\Delta V(x)$ was made exactly equal to $\Delta V(x + a)$ so that output $D(x)$ of the difference amplifier DF (Fig. 2) showed no 20 Hz component. The synchronous switch, operating at 40 Hz, rejected

FIGURE 8 Interstitial currents due to illumination of a small group of rods in a retinal slice. 560 nm stimulus beam of intensity $\sim 10^{11}$ hν cm^{-2} per flash, propagating normal to axes of rods and long axis of slice.

(A) Photograph of slice with electrodes in position and stimulus beam (S) emerging normal to plane of page at electrodes. Geometrical width of slit-shaped beam cross-section was about 6 μm but it was diffused in traversing the layer of rod outer segments. Long axis of beam's cross-section is vertical. Tips of rod outer segments at T. Edge of overlying glass plate at E.

(B) Approximate radial and tangential components i_{zz} and i_{yy} of the divergence of the interstitial current at a radial depth of 40 μm in the slice as a function of distance from stimulus to electrodes. No corrections have been applied for the finite spacing of the electrode arrays. Each point is the average of 16 responses with standard errors due to electrode noise shown. The component of divergence i_{xx} parallel to the stimulus beam was negligible.

(C) Divergence $(i_{zz}+i_{yy})$ of the interstitial current at a radial depth of 40 μm (points) as a function of distance from the center of the stimulus beam to the electrodes. Line: Photometric scan across image of a print of Fig. 8 A developed to contrast $\gamma = 1$. The agreement of current and light distributions is within the ± 10 μm error of the method.

voltage transients produced by the rise and fall of the current pulses. This refinement greatly increased the sensitivity and stability of the measurements. Thus

$$\Delta V(x) = \Delta V(x + a) = I\rho a, \tag{5}$$

where ρ is the resistivity of the bathing fluid. As a test of the uniformity of transretinal current flow, the electrode assembly was then moved ± 100 μm in the Y direction and in the Z direction to the upper and lower surfaces of the slice. At each position, $\Delta V(-35)$ and $\Delta V(-20)$ were measured. Preparations which showed variations of more than 15% were rejected as having a nonuniform distribution of radial current.

The electrode triplet was next inserted radially into the retina until the center electrode B was 40 μm beyond the rod ends at a level about halfway between upper and lower faces of the slice. Since the retinal resistance was larger than that of the Ringer, the new voltage differences $\Delta V(25)$ and $\Delta V(40)$ were larger than $\Delta V(-35)$ and $\Delta V(-20)$. The values K_1 and K_2 of attenuators K_1 and K_2 were accordingly adjusted so that

$$K_1\Delta V(25) = \Delta V(-35) \tag{6 a}$$

$$K_2\Delta V(40) = \Delta V(-20). \tag{6 b}$$

Thus, from equations 4 and 2 the average radial resistances $\bar{r}_x(x_1)$ between planes $x = x_1$ and $x = x_1 + a$ were

$$\bar{r}_x\,(25) = \frac{\rho}{K_1} \tag{7 a}$$

$$\bar{r}_x\,(40) = \frac{\rho}{K_2} \tag{7 b}$$

With the electrodes in position, the stimulus was applied to the slice at each of six horizontal positions beginning at the electrodes and moving away from them in 10 μm steps parallel to the Y axis.

The approximate radial divergence i_{xx} was calculated from the average voltage differences $\Delta V_L(x)$ produced by 16 flashes at each stimulus position, by the relation

$$a^2 i_{xx} \approx \Delta_x(\bar{g}_{xx}\Delta_x V) = K_1\Delta V(x) - K_2\Delta V(x + a) \equiv D(x), \tag{8}$$

where Δ_x indicates differencing with interval a in the X direction and $\bar{g}_{xx} = 1/\bar{r}_x$. The mean peak amplitudes of the light-induced transients in $D(40)$ are plotted in Fig. 8 B vs. horizontal distance along the slice from the line of the electrodes to the center of the stimulus beam. i_{yy} and i_{zz} were next measured by replacing the electrode triplet with their tips at the same 40 μm of radial depth but separated by

15 μm spacing in a line parallel to the Y axis or to the Z axis. The stimuli were repeated at the same positions along the slice. i_{yy} and i_{zz} were calculated from relations analogous to those of equation 7 in which the conductances $\bar{g}_{yy}$ and $\bar{g}_{zz}$ were assumed equal, for lack of more exact figures, to the mean of radial conductance $\bar{g}_{xx}$ between planes $x = 25$ and $x = 55$. i_{yy} is plotted vs. stimulus beam position in Fig. 8 B. No curve for i_{zz} is shown, because values were negligibly small in the slice at all beam positions.

The sum of i_{xx} and i_{yy}, which by equation 2 *a* is an estimate of i_m, is plotted in Fig. 8 C together with a photometric scan of Fig. 8 A at the 20 μm level of the receptor layer. The agreement between distribution of light and current are within the ± 10 μm error of the method and suggest that *only illuminated rods produce the photocurrents observed in the receptor layer.*

Radial Distribution of the Photocurrent in the Receptor Layer

The signal-to-noise ratios in responses of locally illuminated slices were too low or the required number of measurements too many to permit the complete radial distribution of i_m to be accurately measured. But if a slice was uniformly flooded with light, the radial voltage gradients were much larger while the gradients along the Y and Z directions became negligible. Thus, membrane currents of the radially disposed cells could be inferred directly from radial voltage gradients alone. Fig. 9 shows an example of this spatial uniformity. Electrode A was placed at the rod tips at a point with x, y, z coordinates (0, 0, 100) about halfway between the Z planes bounding the upper and lower cut faces of the slice (coordinates in μm). Electrodes B and C were inserted into the layer of receptor nuclei to points (70, 100, 100) and (70, 200, 100). Thus, their tips were both about 70 μm deep but 100 μm apart. 16 flashes of wavelength 560 nm and energy 1.5×10^{11} hν cm^{-2} were given. The average voltage transients $V_A - V_B$ and $V_B - V_C$ show that a large radial voltage

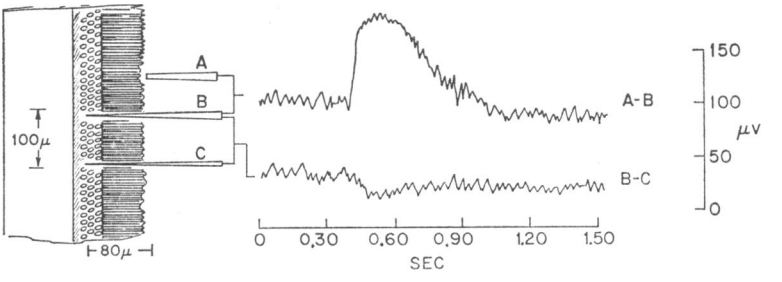

FIGURE 9 Spatial uniformity of photovoltage along a uniformly illuminated slice. Electrodes B and C inserted to a depth of *circa* 80 μm into center of slice. Electrode A at rod tips. Stimulus: 560 nm flashes of intensity 1.5×10^{11} hν cm^{-2} to entire slice. Although there was an 80 mv response recorded between A and B, electrodes B and C, which were 75 μm apart, recorded virtually the same photovoltage. Radial movement of C by ± 5 μm reversed the sign of the transient in B–C.

gradient was produced by the light, but the gradient in the Y direction was small. The deflection in $V_B - V_C$ could be completely eliminated by an adjustment of ± 5 μm in the radial depth of either electrode and thus could be due entirely to errors in electrode placement. Thus, the uniformity condition apparently held.

Placing the electrodes in a vertical line parallel to the direction of propagation of the stimulus also showed the gradients in the Z direction to be negligible so long as the stimuli were not too strongly absorbed by the rods. Hence, 560 nm stimuli which are only 50% absorbed by a 200 μ slice were always used rather than shorter wavelengths which are more efficient in producing rod responses, but which are almost totally absorbed in the upper layers of the slice.

As a check of the effect of the microelectrodes on the preexisting interstitial voltage gradient (the objectivity condition), the response of a slice was recorded with two electrodes A and B at (0, 0, 0) and (100, 0, 0). A third electrode, C, was then inserted into the retina at (100, 0, 30) and the response remeasured. The third electrode was not found to affect $V_A - V_B$ by more than $\pm 10\%$.

Records of $D(x)$ vs. time after 1 μsec flashes of intensity 1×10^{11} hν cm^{-2} for several radial depths of an electrode triplet are shown in Fig. 10. The traces were recorded by the procedure described in the preceding section using 16 repetitions of the stimuli. Note that the noise levels are less at the deeper electrode positions, because the retinal resistance was higher there and the attenuating factors K_1 and K_2 were therefore smaller. Although i_{zz} changed sign as the receptor layer was traversed, the shapes of the waveforms were unchanged, as if all were produced by the same temporal process.

Plots of $D(x)$ vs. radial depth for three uniformly illuminated slices are shown in Fig. 11. In each case 10 μm intertip spacings of the electrode triplet were used and

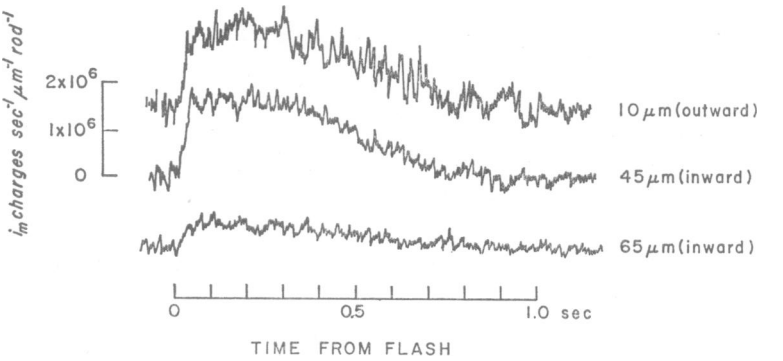

FIGURE 10 Waveforms of rod membrane photocurrent vs. radial depth in receptor layer, as measured by second space differences of extracellular potential recorded with three electrodes. Curves recorded with center electrode at 45 and 65 μm indicate inward current there, but they have been inverted to show their similarity in shape to the outward current waveform recorded at a depth of 10 μm. Each curve is the average of 8 responses. Stimulus: 1 μsec flashes of energy 10^{11} hν cm^{-2} (560 nm).

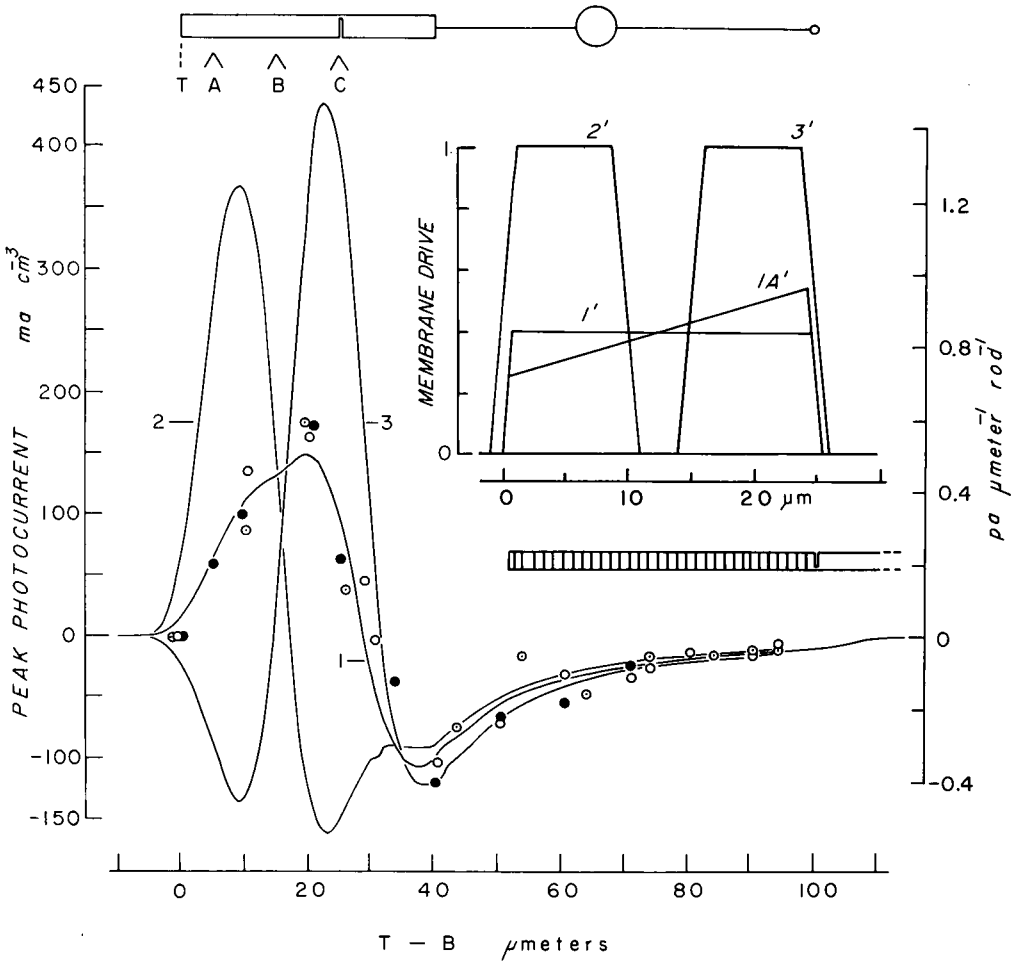

FIGURE 11 Radial component $D(x)$ of divergence of interstitial current in uniformly illuminated slices.
Points: Peak values of $D(x)$ for slices illuminated with 560 nm of flashes of intensity 2×10^{10} $h\nu$ cm^{-2} (filled circles) or 8×10^{10} $h\nu$ cm^{-2} (open and dotted circles). All responses scaled to amplitudes which would have been obtained for saturating flashes ($>2 \times 10^{11}$ $h\nu$ cm^{-2}). Curves: Theoretical values of $D(x)$ to be expected from a layer of model rods with membrane drive current distributions shown in the inset and scanned with a triplet of microelectrodes with radial intertip spacings of 10 μm. See text.

16 traces were summed in the signal averager at each position of the electrode triplet. The filled circles represent a slice illuminated with flashes of intensity 2×10^{10} $h\nu$ cm^{-2} while the open and dotted circles are from two slices exposed to flashes four times more intense. By using the amplitude:intensity relation for each slice, all responses were scaled to the amplitudes they would have shown had the stimuli been of saturating intensity ($\sim 2 \times 10^{11}$ $h\nu$ cm^{-2}).

Fig. 11 also shows plots of theoretical curves of $D(x)$ derived from solutions of the cable equation for a model rod layer (Appendix II) scanned with an electrode triplet with 10 μm intertip spacings. Curve 1 was computed for hypothetical rods with a uniform membrane conductance G_m per unit area of outer segments, inner segments, and cell bodies and possessing constant current generators uniformly distributed along the plasma membrane of just the outer segments (inset, curve 1'). The computed curve was adjusted to a least-squares fit by simultaneously varying the strength ϕ of the membrane source current and the conductance G_m of the entire cell membrane. The optimum values were $G_m = 8.2 \pm 2.3 \times 10^{-3}$ mho cm^{-2} and $\phi = 7.9 \pm 2.2$ μa cm^{-2}, both values being expressed per unit area of rod plasma membrane. The stated uncertainties are standard errors of the estimates due to the residuals. Curves 2 and 3 are calculated for hypothetical current generators confined to the outer and inner 10 μm of the outer segments. Neither can be made to fit the observations with any values of ϕ and G_m . However, other source current distributions which conform to the data are possible. For example, the distribution of curve 1A', in which there is a two-fold increase in drive current from tips to bases of the outer segments yields a good fit with virtually the same values of ϕ and G. By trying other distributions it was found that the essential feature of a good fit was always a membrane source current which is relatively uniform per unit of radial depth in the receptor layer but whose sign changes at the junction between inner and outer segments.

The computed curves show small irregularities, particularly between 20–40 μm. As explained in Appendix I, these are not computational errors. They arise from the finite spacing of the electrode arrays. Thus, they can be taken to indicate the maximum accuracy of the experimental method for estimating the spatial distribution of rod membrane currents.

While the good fit of curve 1 to the points in Fig. 11 gives an accurate picture of the radial distribution of current generators in the cell membranes, the estimate of G_m is relatively inaccurate and should only be taken as an upper limit to the true value. In the curve fitting process, G_m is determined mainly by the measured density of rod membrane current in the nuclear and synaptic regions (x = 50–100 μm) relative to that in the outer and inner segments and by the distribution of membrane area and cytoplasmic resistance between 50 and 100 μm. Each of these factors may be subject to two-fold error. Nor is it known that G_m is independent of x, as was assumed in the computations. Nevertheless, it will be seen that the high estimate of G_m (which predicts a membrane time constant of only 10^{-4} sec) is still low enough to allow the observed photocurrent to produce significant changes in membrane potential at the rod synapses.

Radial Distribution of the Dark Current

While the dark current distribution can also be investigated by the three electrode method, in principle, results were not generally satisfactory because of DC drift in

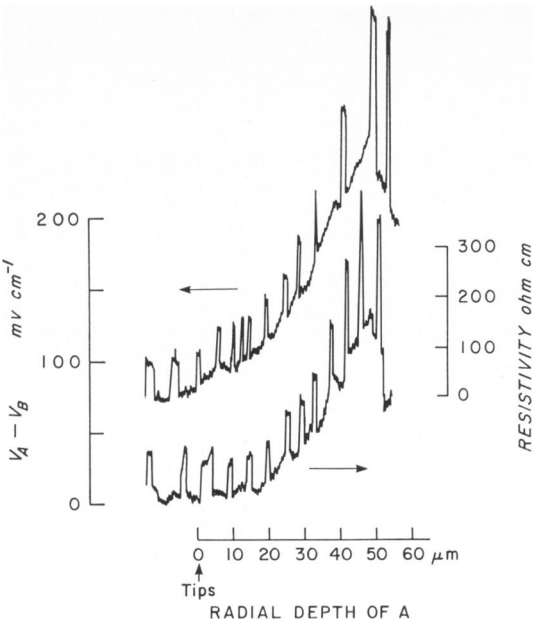

FIGURE 12 Radial dark voltage gradients in rod layer of a retinal slice. Voltage differences beteen a pair of micropipettes (A, B) with 10 μm radial spacing is plotted against depth of the deeper electrode (A). Records of an insertion and withdrawal are shown spaced apart vertically for clarity. Induced square voltage transients are due to pulses of radial current applied from external electrodes.

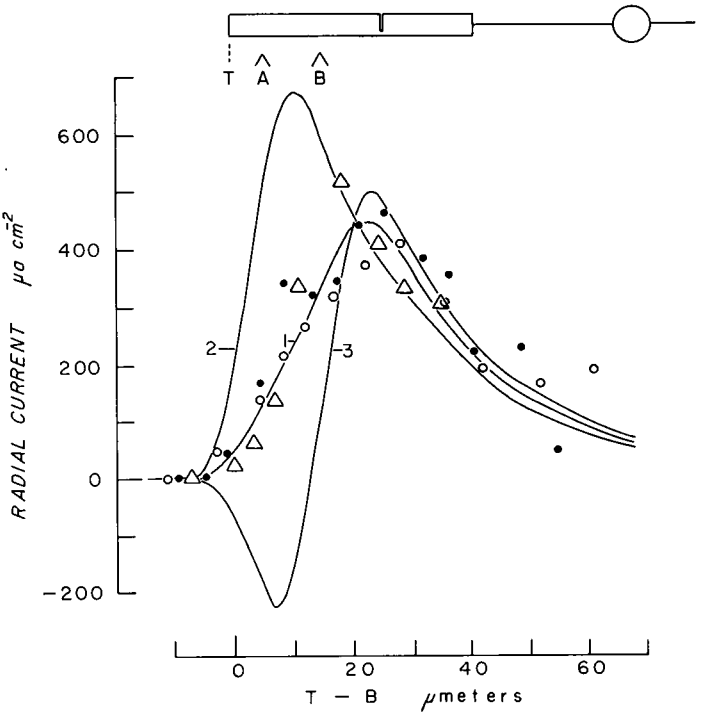

FIGURE 13 Radial distribution of dark current.
Points: Radial currents calculated from data like that of Fig. 12 for three slices in Ringer II.
Curves: Theoretical distributions of radial current calculated from drive current distributions 1′, 2′, and 3′ of Fig. 11 with the sign of the membrane drive current reversed and its amplitude adjusted to fit the points.

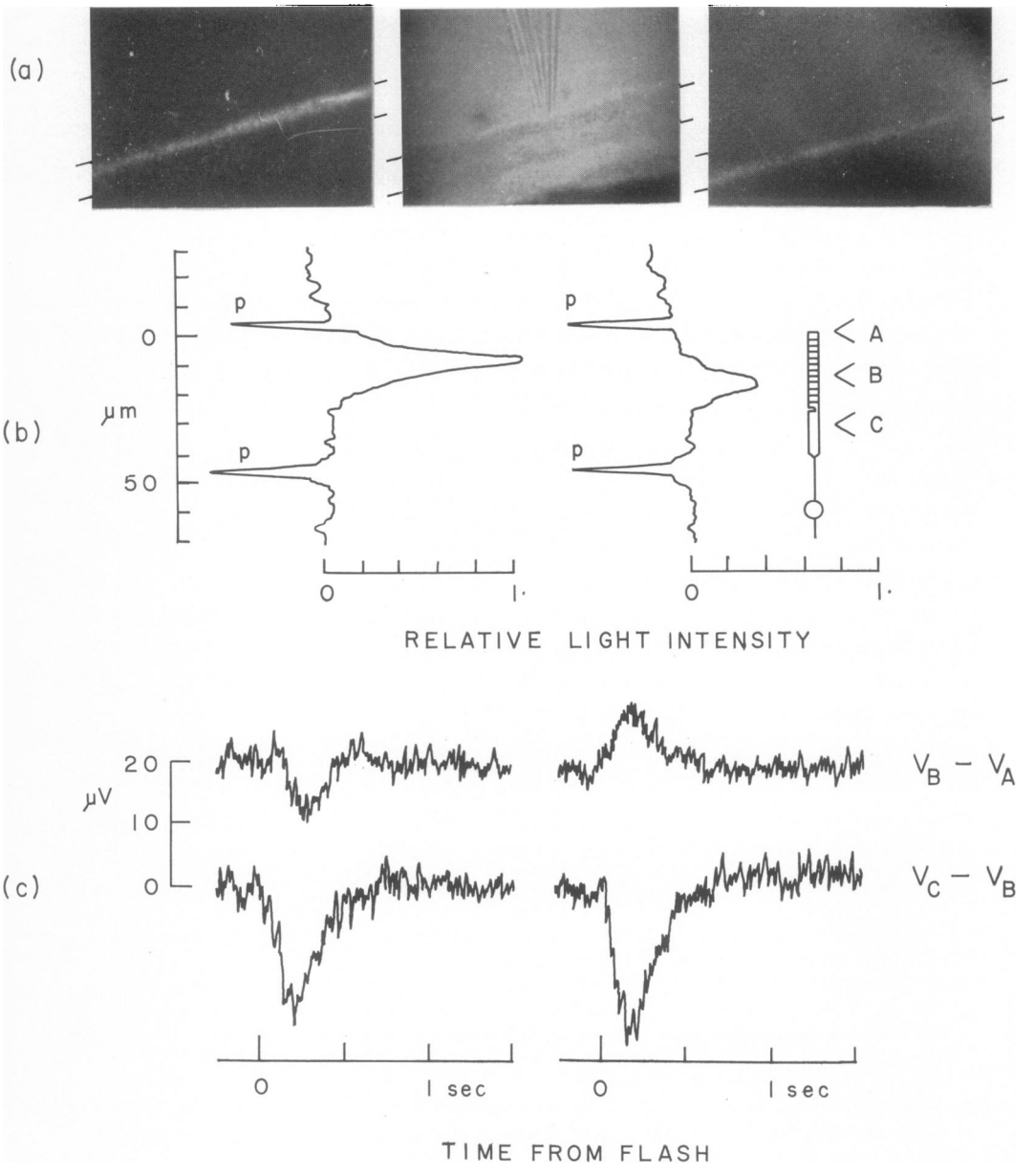

FIGURE 14 a, b, c.

the recording electrodes during the 15–20 min required for a complete set of radial measurements. Another method based on two electrodes was therefore used. Two pipettes with a 10 μm radial intertip spacing were thrust radially through the receptor layer to a depth of 100 μm and then slowly withdrawn. Simultaneously, radial current pulses were applied across the slice and the voltage difference between the electrodes was displayed as the Y displacement on an X-Y plotter. The radial displacement of the electrode pair was measured by a directly coupled linear variable differential transformer, whose amplified output generated the X displacement of the plotter. With this arrangement a complete resistance and voltage profile (Fig. 12) could be measured in less than 20 sec. The leading electrode was always positive relative to the trailing one, with the greatest voltage difference occurring at a depth of about 40 μm. The retinal resistance was increasing steeply at this point, however, as can be seen from the rapid change in the height of the voltage transient induced by the applied currents. The radial current i_x thus reached a maximum at a depth of about 25 μm. Fig. 13 shows this for three different slice preparations. In each, as in almost all slices in Ringer II, the dark voltage gradient had a uniform profile with a single maximum at the junction between inner and outer segments, indicating that the membrane dark current reverses sign there. The calculated maximum radial current was also remarkably constant. Ten slices yielded an average current of 32.5 $\pm$ 5.2 (SD) pa per rod with a range of 18–44 pa.

Fig. 13 also shows theoretical values of i_x calculated for the hypothetical membrane drive current distributions of Fig. 11. The curves are simply the space integrals of the latter. Curve 1 corresponds to a uniform current distribution on cells with the same membrane parameters as those of Fig. 11. Only one parameter, the drive current I_D was varied to fit curve to points. It is clear that the nonuniform distributions of curves 2 and 3 fit the data no better than do the corresponding curves of Fig. 11 for the photocurrent. Thus, while the dark current through the rod membranes in Ringer II is relatively larger and is opposite in sign to the membrane photo-

---

FIGURE 14 Effect of local illumination of radial zones in rod outer segments on the distribution of radial interstitial current of a retinal slice.

(*a*) Infrared photomicrographs of slice with electrode triplet inserted in receptor layer (center). Stimulus beam crossing outer segments near their tips (left) and near their bases (right). Stimulus: 10 msec flashes from tungsten lamp filtered through Kodak Wratten No. 70 filter transmitting wavelengths >640 nm. Energy equivalent to 10^{11} hν cm^{-2} at 560 nm. Diagonal lines indicate tips of rods and approximal boundary of inner segments (distance 40 μm).

(*b*) Photometric scans across stimulus beam as it emerged from slice in position near tips of outer segments (left) or near bases (right). Intensity scale is approximately linear. Graticule lines on scanning microdensitometer at p.

(*c*) Voltage differences between adjacent pairs of electrodes at two positions of stimulus slit. Reversal of V_A-V_B with shift of stimulus indicates that source of photocurrent moves with the light. Each curve is mean of response to 32 flashes.

current, it has essentially the same radial distribution. That is, it flows *inward* along the outer segments and *outward* along the inner segments, cell bodies, and synaptic terminals.

In Ringer I the radial interstitial dark voltage gradient was similar to that in Ringer II at depths of 0–40 μm. Deeper in the receptor layer, however, the gradient often reversed, as if there were sinks for the dark current at the synaptic ends of the rod as well as in the outer segments. Because of this added complexity, only Ringer II was used in most experiments.

Effect of Local Illumination on the Radial Distribution of the Photocurrent

While diffusely illuminated outer segments produce a relatively uniform source of outwardly directed membrane photocurrent, the source distribution can be made nonuniform by local illumination. If a 100 μm thick slice was illuminated with flashes in the form of a beam with a slit shaped cross-section perpendicular to the rod axes and focused on the outer half of the outer segments (Fig. 14 *a* and *b*, left), radial voltage gradients such as those in Fig. 14 *c*, left, were obtained. Three electrodes, A, B, and C, were placed at radial depths of 0, 15, and 30 μm and the voltage differences ΔV_1 ($= V_A - V_B$) and ΔV_2 ($= V_B - V_C$) were simultaneously recorded on two channels of an FM tape recorder. The average photovoltage transients to 32 successive red flashes were of outer-segment–positive sign in both ΔV_1 and ΔV_2. This would be expected if an outward drive current were produced over any appreciable region of the outer segments between electrodes A and B in a layer of model rods (cf. curves 1 and 2 of Fig. 13). When the stimulus slit was moved radially inward until it covered the inner half of the outer segments (Fig. 14 *a*, *b*, right), ΔV_1 reversed sign while ΔV_2 was almost unchanged (Fig. 14 *c*, right). For this case, the membrane current source apparently moved with the light (cf. Fig. 13, curve 3). In 20 repetitions of the experiment on other slices, the same result was obtained in six cases, while in six cases ΔV_1 did not reverse sign at the deeper stimulus position but became smaller. Since this would occur if the stimulus beam were not exactly focused or were diffused excessively, such failures are to be expected. In the remaining eight tries, the slices failed to give stable photocurrents throughout the experiments. Thus, it can be concluded that (*a*) *the photocurrent is generated primarily in zones of an outer segment which are illuminated* and that (*b*) *unilluminated zones of the outer segments, like the rest of each rod cell, act as sinks for the photocurrent.*

DISCUSSION

Site of the Action of Light

The mode of signal transmission along vertebrate photoreceptors has long been a subject of controversy. Though there is much inferential evidence that the receptor layer produces some components of the electroretinogram (ERG) (see Granit, 1963; Tomita, 1963; Nilsson and Crescitelli, 1969), direct attempts to analyze the intraretinal currents and voltages with extracellular microelectrodes have not produced

clear-cut results. Byzov (1965) has reported that the rods and cones of the frog retina are electrically silent, while Brindley (1956) has placed both the a- and b-wave generators in the receptor layer and Brown and his coworkers (see Brown, 1968) have attributed the a-wave and PIII components of the ERG to current sources at the inner segments with sinks located more proximally near the receptor-bipolar synapses.

Intracellular recording methods together with electrode marking have proved more fruitful. Bortoff (1964), Bortoff and Norton (1965, 1967), Kaneko and Hashimoto (1967), and Werblin and Dowling (1969) have established that cones, at least, are hyperpolarized in a graded way by light and that the waveform of the responses resemble the PIII component of the ERG. But these results do not indicate whether light's action on cone membrane potentials is a primary one or a secondary phenomenon due to a synaptic feedback from deeper retinal neurons in which the receptors respond as postsynaptic elements. The present experiments do not entirely exclude synaptic feedback. Computations on a model rod with a current generator in the presynaptic membrane show that a feedback current generated at a rod synapse could cancel the presynaptic effect of a photocurrent 40 times larger. Such a small feedback current would be invisible with the present technique. But it seems clear that light's major effect in rat rods is to reduce a large standing membrane current which is inward at the outer segment and outward along the remainder of each cell.

By itself, this result cannot be taken as proof that light's current-controlling effect takes place in the outer segments, because the same radial distribution of the membrane current could be produced by inwardly directed light-activated current generators along the cell bodies, by outwardly directed ones in the outer segments, or by a combination of the two. Since locally illuminating the outer segments produces a relatively local outward photocurrent, however, it is reasonable to place light's primary electrical action there and to assign a passive electrical role to the remainder of the plasma membrane.

Signal Transmission by the Photocurrent

Is the photocurrent large enough to explain the well-known ability of retinal rods to count single absorbed photons (Hecht, Shlaer, and Pirenne, 1942)? If so, an absorbed photon must produce a disturbance of the rod's presynaptic membrane potential (a "*QR*") which is at least large enough to be recognized in the presence of the thermal noise of the membrane impedance. For cells the size of vertebrate rods, this means that a photon-activated current generator in an outer segment must produce a minimum flow of several hundred electronic charges through the plasma membrane even if cable losses are small (Hagins, 1965). But if the values of cable parameters for rat rods obtained from the present experiments are roughly correct, losses are so great in passive signal transmission that this minimum charge flow is a

serious underestimate of what is actually required to produce a detectable membrane potential displacement at the rod's synapse. Thus, it is instructive to consider if an ideal detecting device located at the presynaptic membrane of a rod with the electrical parameters actually obtained could detect QR's originating in the outer segment. Such a detector might be thought of as a linear frequency-selective filter (an "optimum linear filter") followed by a threshold device which responds whenever the filter output exceeds a fixed level.

Since the mean space constant λ of the rod fiber near the synapse is given by

$$\lambda = (RG)^{-1/2} \approx 25\ \mu\text{m},$$

the presynaptic terminal is about 2λ from the inner segment and can be treated in noise calculations as if it were at one end of a semi-infinite cable. The characteristic impedance Z_o at frequency $\omega = 2\pi f$ of the cable is (see Terman, 1943, p. 173)

$$Z_o = (R_z/[G_m + j\omega C])^{1/2}.$$

Thus, by Nyquist's theorem (Lawson and Uhlenbeck, 1950, p. 74) the spectrum $\overline{v^2}$ of the membrane voltage fluctuations at the synapse is

$$\overline{v^2}(f) = 4k\text{T}(\text{Real Part of } Z_o)$$

where k is Boltzmann's constant and T is the absolute temperature. If $C = 1\mu\text{F}$ cm^{-2}, as is the case for most cells (Cole, 1968), the rod membrane time constant (C/G_m) is 10^{-4} sec, and Z_o's real part is essentially constant from $f = 0$–1000 Hz for the rod's synaptic terminal. But an optimum linear filter at the input of a detector of voltage disturbances due to the absorption of single photons will be adjusted to detect only waveforms resembling QR's and so will have a much narrower frequency passband than the membrane noise spectrum. If a QR is of the same form as the photocurrent waveform to a very short flash (e.g. Fig. 6 *g*), it can be described by an equation of the form[1] $t \exp(-bt)$ where b is about 5 sec^{-1} at 33°C.

The optimum filter at the rod synapse will thus have a frequency attenuation factor $A(f)$ (Laning and Battin, 1956, p. 278)

$$A(f) = (1 + [2\pi f/b]^2)^{-2}.$$

The total rms voltage fluctuation in the frequency band admitted by the detector will be no more than 0.9 μv unless additional nonthermal noise sources are also present in the membrane (cf. Derksen and Verveen, 1966).

The size of a QR at a rod synapse can be estimated from the cable parameters, photocurrents, and light-absorbing properties of rods. 560 μm stimuli containing about 1.5×10^{10} $h\nu$ cm^{-2} produced photocurrents of about half-saturating amplitude. Since the absorbance at 500 nm due to rhodopsin in rod outer segments is

about 0.01 μm^{-1} for light traveling parallel to their long axes (Hagins, 1957; Liebman and Entine, 1968), the fraction P of a 560 nm flash incident perpendicular to an outer segment axis which will be absorbed by rhodopsin is about

$$0.01\ \mu m^{-1} \cdot \log_e 10 \cdot \tfrac{1}{2} \cdot (\epsilon_{560}/\epsilon_{500}) \cdot (\pi d/4) = P,$$

where the factor $\frac{1}{2}$ is due to orientation of the chromophores normal to the rod axes, $(\epsilon_{560}/\epsilon_{500})$ $(= \sim 0.28)$ is the ratio of rhodopsin's extinction coefficients at 560 and 500 nm and $(\pi/4)d$ is the mean thickness of a cylinder of radius d. For a 1.7 μm diameter rod, $P \approx 3.6 \times 10^{-3}$ and thus about 27 photons are absorbed from the half-saturating flash, neglecting self screening of rhodopsin due to the relatively great thickness of the slices.

The change in membrane potential at the synapse caused by a flash can be estimated from Fig. 15. The membrane potential V is plotted vs. x for a model rod with a total dark current of 71.8 pa produced by the current generators in the outer segment membrane and a saturated photocurrent which is half the dark current. In darkness $V - V_m$ (solid curve) declines from about 4 mv at the distal end of the outer segment to 320 μv at the synapse. Exposure to a flash of 1×10^{11} hν cm^{-2} produces a photocurrent response of saturating amplitude which reduces $V - V_m$ to about 2 mv at the outer segment and 160 μv at the synapse (dashed curve). Since

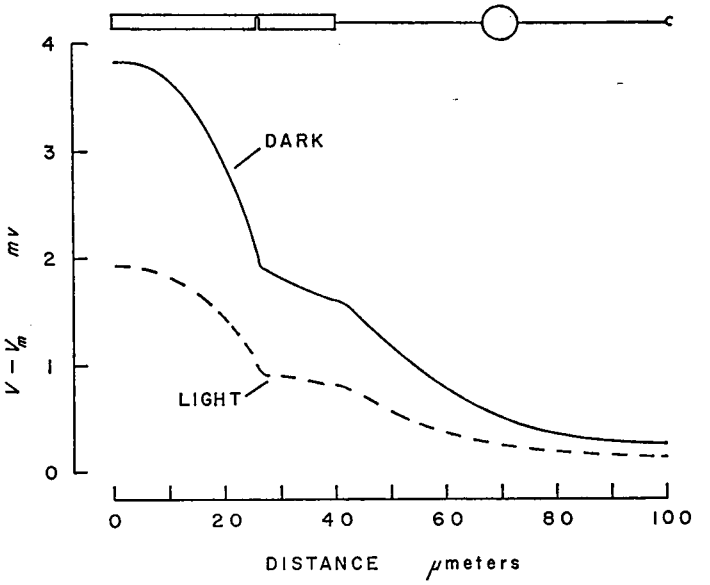

FIGURE 15 Displacement of membrane potential of a rat rod from its resting value V_m in the absence of both dark current and photocurrent by dark current (solid line) and by combined dark current and saturating photocurrent (dashes). Computed for a model rod with membrane conductance $G = 9.7 \times 10^{-3}$ mho cm^{-2} and membrane drive current ϕ of 58 μa cm^{-2} in dark and 29 μa cm^{-2} in light. See Appendix II.

the voltage displacement was related to flash energy by equation 4, the voltage increment to a single absorbed photon would be about 6 μv at the input to the linear filter or about 3.6 μv at its output, a figure four times the rms membrane noise. With this signal-to-noise ratio, an ideal detector responding to maxima greater than a certain fixed threshold level in the output of the filter could perform with a rate of false positive photon responses of less than 1 per 100 sec and a negligible rate of false negatives (see Rice, 1954, part III, sects. 3.3 and 3.6). By comparison, Barlow (1957) estimates from frequency-of-seeing experiments that human rods might produce false positive responses every 10–50 sec.

Thus, the photocurrent produced by rat rods is large enough to permit single photon detection with a small safety margin even with the short space constant and high membrane conductance found for rat rods in our experiments.

Nature of the Photoelectric Transducer

Like the QR's of squid photoreceptors, the responses of rat rods show a large quantum current gain. If every absorbed photon produces a QR of the form $t\exp(-5.0t)$, a flash causing 27 photons to be absorbed per rod in the slices of Fig. 14 yielded interstitial currents which require the photocurrent generators in the outer segment to produce about 15 pcoul or 2.3×10^6 electronic charges per photon. Clearly such a large current gain is outside the usual realm of photoconduction in solids, but it is well within range of what can be accomplished by membrane permeability changes. If the driving force for the photocurrent is E volts, the peak drive current of 18 pa produced by a rod excited with 27 absorbed photons (Fig. 11) could result from elementary photon-induced conductance changes g of about $0.5/E$ pmho. While E is not known, it cannot be less than about 5 mv because the drive current distribution is almost uniform along the rod outer segments despite a calculated variation in membrane potential of at least 2 mv in passing from tips to bases. Thus, an elementary conductance change g in the plasma membrane of the outer segments need not be greater than about 100 pmho to explain the photocurrent. This figure is similar to the value of $\sim$20 pmho derived for squid photoreceptors (Hagins, 1965).

Significance of the Dark Current

The existence of a standing voltage gradient in the interstitial space of the receptor layer has been hinted at in the past (cf. Granit, 1963), mainly to explain the potential difference between vitreal and scleral surfaces of an excised eyecup. This conclusion is indirect, because the pigment epithelium shows a voltage difference of its own between its two surfaces (Lasansky and de Fisch, 1966) so that it is difficult to estimate the specific contribution of the receptors in older work. However, Svaetichin, Negishi, and Fatechand (1965) reported briefly a microelectrode penetration study from which they concluded that the receptor layer of an isolated fish retina, when

treated with NH_3 vapor, shows a 5 mv potential difference between receptor tips and synapses, the receptor tips being relatively negative.

The present experiments indicate that the voltage gradient in the interstices between rods of the rat retina under physiological conditions is caused by a steady flow of radial current so large as to have important metabolic consequences, at least in Ringer II. This can be seen from the calculations summarized in Table III.

The short turnover time for ions agrees with the rapid action of CN^- in suppressing both dark current and photocurrent. The calculated Q_{O_2} is somewhat larger than the values of 10–30 found by conventional respirometry (Altman and Dittmer, 1968, pp. 391–2), but the difference can be put to errors in the parameters used in Table III, on one hand, and to the rough treatment accorded the retinas used in most metabolic studies, on the other.

Why does the dark current exist? Three possible explanations occur to us. It might be an abnormal phenomenon due to mistreatment of the isolated retina, it

TABLE III

METABOLIC CONSEQUENCES OF THE DARK CURRENT

Calculated for a retina with a radial interstitial dark current of 705 μa cm^{-2} at the inner-outer segment junctions

		Notes
A. Equivalent membrane drive current to produce observed radial dark current	71 pa rod^{-1}	
B. Equivalent univalent ionic membrane flux	7.4×10^{-16} mole sec^{-1} rod^{-1}	
C. Ionic composition of receptors		
Rod volume	3.3×10^{-10} cm^3	*
Water content		
25 μm outer segment	60%	‡
75 μm cell body, etc.	82%	§
Weighted mean	76.5%	
Rod water	2.5×10^{-13} liter rod^{-1}	
Total cations	3.5×10^{-14} mole rod^{-1}	‖
D. Turnover time for cell cations	47 sec	¶
E. Energetic requirements to sustain the dark current		
ATP consumption	2.5×10^{-16} mole rod^{-1} sec^{-1}	**
O_2 consumption	4.1×10^{-17} mole rod^{-1} sec^{-1}	‡‡
Q_{O_2} of rod layer	51 mm^3 O_2 (mg dry wt)$^{-1}$ hr^{-1}	

* Müller cell processes counted as part of rods.

‡ Based on a refractive index of 1.40 (Sidman, 1957), and a refractive increment for lipoproteins of about 0.16 cm^3 g^{-1} (Davies, 1958).

§ See Altman, P. L., and D. S. Dittmer (1961), p. 326.

‖ Assuming cell water is 0.14 M in cations.

¶ Assuming all cations participate in current.

** Assuming 3 univalent cations pumped per ATP hydrolyzed (Caldwell, 1968).

‡‡ Assuming 6 ATP's produced per O_2 consumed in oxidative phosphorylation.

might serve as DC signal carrier which is modulated by resistance changes in the outer segment, or it might act to transport materials in the receptor cytoplasm by electrophoresis. The first of these is unlikely because the dark current persists for many hours under a variety of conditions in frog as well as rat retinas (unpublished observations). Moreover, vertebrate photoreceptors contain an unusually large number and high density of mitochondria compared to other nerve cells, as if a heavy metabolic load were usual in the living eye.

The idea that the dark current is a DC signal carrier is more attractive. It fits well with the observation that photocurrent of saturating amplitude reduces the radial interstitial current but does not reverse it, and with the report by Toyoda, Nosaki, and Tomita (1969) that light increases by 1–3 MΩ the resistance between a pipette tip inside a cone and an external electrode. But neither observation is compelling; I_x may well reverse under other conditions we have not explored, while the reported resistance changes have not yet been definitely shown to arise in the plasma membranes of the outer segments or to be adequately large to explain the size of the photocurrent. A more serious difficulty stems from the question of why the dark current is so large. In principle, the signal gain of an amplitude-modulated signal-carrier system is proportional to the carrier amplitude, so that the larger the dark current, the larger the effect at the synapse of a given conductance change in the outer segment. But since the necessary condition for signal transmission is only that *QR*'s must produce voltage changes at the presynaptic membrane which exceed thermal noise, this could be accomplished by increasing the cell membrane resistance of the rod from its estimated value of about 100 Ω cm² to the 10,000 Ω cm² characteristic of some neurons (Cole, 1968). With a ten-fold higher membrane resistance, the presynaptic membrane potential could be displaced by three times the thermal noise level with a photocurrent nearly 100 times weaker than that actually produced in a *QR*. A correspondingly small dark current would therefore be needed. The overall electrical efficiency of the transmission process could thereby be greatly increased at a much smaller energy cost to the receptors.

The only definitive effect which a large dark current can produce but a small one cannot is a larger longitudinal voltage gradient inside and outside the receptors. The external gradient is small, of course, because the interstitial resistance is low, but inside a rod outer segment and at the incisure the gradient may exceed 3 v cm^{-1}. For the model rod of Fig. 15, the internal voltage gradient is sufficient to produce a 20% increase in equilibrium concentration at the rod tip of a trivalent negative ion (such as ATP at pH 7) relative to its concentration at the 40 μm level of the inner segment. While this is a small effect, a protein molecule with a net charge of −16 would be distributed with a 3:1 concentration ratio under the same conditions. It remains for future work to weigh the possible significance of such longitudinal potential fields in the growth (Young, 1967) and metabolism of vertebrate rods and cones as well as in transmission of sensory signals.

We thank Dr. Mones Berman and Mrs. Marjory Weiss for advice about the computations and Mr. Charles Hanna for the electron micrographs.

Received for publication 13 October 1969.

APPENDIX I

Effect of Finite Electrode Spacing on Estimates of Currents and Divergences

Consider three electrodes spaced in a radial line at points $(x - a, 0, 0)$, $(x, 0, 0)$ and $(x + a, 0, 0)$ in a rectangular coordinate system.

The potential $V(x, 0, 0)$ is

$$\int_{-\infty}^{x} i_x(\xi) r_{xx}(\xi)\, d\xi, \qquad (1[AI])$$

where the integration is along the x axis.

Then,

$$\Delta V(x) \equiv V(x - a, 0, 0) - V(x, 0, 0) = \int_{-a}^{0} i_x(x + \xi) r_{xx}(x + \xi)\, d\xi. \qquad (2[AI])$$

The voltage difference between planes $x - a = 0$ and $x = 0$ divided by the mean resistance between planes is

$$i_x' \equiv \Delta V(x) \Big/ \int_0^a r_{xx}(x - a + \xi)\, d\xi = \int_{x-a}^{x} i_x(\xi) w(x, \xi)\, d\xi, \qquad (3[AI])$$

where

$$w(x, \xi) = r(\xi)/\bar{r}(x)$$

and

$$\bar{r}(x) = (1/a) \int_0^a r(x - a + \xi)\, d\xi.$$

Thus $\bar{i}_x'$ is the radial current i_x averaged over interval $(x - a, x)$ with weighting function $w(x, \xi)$.

If

$$\sigma(x, \xi) = (r[\xi] - \bar{r}[x])/\bar{r}(x), \qquad (4[AI])$$

then

$$D(x)\bar{i}_x'(x) - \bar{i}_x'(x + a) = \bar{\bar{J}} + \psi, \qquad (5[AI])$$

where

$$\bar{\bar{J}} = \left[\frac{\partial}{\partial x} \left(g_{xx} \frac{\partial V}{\partial x} \right) \right]^{**}, \qquad (6[AI])$$

and each asterisk indicates an averaging operation, i.e.

$$F(x)^* \equiv (1/a) \int_{-a/2}^{+a/2} F(x + \xi)\, d\xi. \qquad (7[AI])$$

Thus, $D(x)$ differs from the second-order average $\bar{J}$ of the radial component of current divergence by a correction term ψ, where

$$\psi = (1/a) \left[\int_{x-a}^{x} i_z(\xi)\sigma(x - a, \xi)\, d\xi - \int_{x}^{x+a} i_z(\xi)\sigma(x, \xi)\, d\xi \right]. \qquad (8[AI])$$

The relative contributions of $\bar{J}$ and ψ to $D(x)$ for the model rod of Figs. 11, 13, and 15 were calculated (Appendix II). In no case did $\psi(x)$ exceed 5% of the largest value of $\bar{J}$. ψ's contribution was evident, however, as the small irregularities in the curves of Fig. 11 in the interval 20–40 μm. Thus, for electrode spacings of 10 μm, $D(x)$ is a good approximation to $\bar{J}$.

APPENDIX II

Steady-State Solution of the Cable Equations for a Retinal Photoreceptor

In a uniformly active mosaic each cell was treated as a noninductive coaxial electric cable, the two longitudinal conductors being the cell's cytoplasm and that part of the interstitial space enclosed by a hexagonal prism comprising one elementary unit of the mosaic. The voltages and currents in the receptor layer are thus given by the solution of a one-dimensional boundary value problem. If the plasma membrane is approximated by a linear conductance $G(x)$ in parallel with a constant current generator $\phi(x)$, the net membrane current density at x is

$$I_m = GV_m + \phi. \qquad (1[AII])$$

The cable equation is thus

$$\frac{d}{dx}\left[\frac{1}{R_E + R_c}\frac{dV_m}{dx}\right] - GV_m - \phi = 0, \qquad (2[AII])$$

with boundary conditions

$$\frac{dV_m}{dx} = 0 \quad \text{at} \quad x = 0 \quad \text{and} \quad x = L. \qquad (3[AII])$$

Equation 2 was approximated by 400 difference equations for the voltages at equal space intervals along the cell. The system was solved by a standard method and Richardson's corrections were applied (Wachpress, 1960). The fractional errors in V_m due to the finite difference approximations were less than 10^{-6}.

The voltages along the interstitial space were calculated from the approximation

$$V(x) \approx \sum_{j=1}^{J-1} \beta_j \Delta V_{mj} + \theta\beta_J\, \Delta V_{mJ} \qquad (4[AII])$$

where

$$\beta_j = \bar{R}_{Ej}/(\bar{R}_{Cj} + \bar{R}_{Ej}), \qquad \theta = (x/h) - J + 1,$$

h is the space step size, and

$$\bar{R}_{Ej} = (1/h) \int_{hj}^{h(j+1)} R_E(x)\, dx, \quad \text{etc.} \qquad (5[\text{AII}])$$

Next, $D(x)$ was computed for the model using equation 7 and the values adjusted to those observed in the experiments by a linearized least-squares procedure (Guest, 1961, sect. 10.2) with two parameters adjustable during each iteration. In each case the calculations were repeated with the same results for at least four different initial estimates for each parameter. Only final estimates derived from well-behaved parabolic minima in the sums of squares of the residuals were accepted.

REFERENCES

ALTMAN, P. L., and D. S. DITTMER. 1961. *In* Biological Handbooks: Blood and other Body Fluids. Federation of American Societies for Experimental Biology, Washington, D. C. 326.

ALTMAN, P. L., and D. S. DITTMER. 1968. *In* Biological Handbooks: Metabolism. Federation of American Societies for Experimental Biology, Washington, D. C. 391–2.

BARLOW, H. B. 1957. *J. Physiol. (London).* **136**:469.

BORTOFF, A. 1964. *Vision Res.* **4**:627.

BORTOFF, A., and A. L. NORTON. 1965. *Vision Res.* **5**:527.

BORTOFF, A., and A. L. NORTON. 1967. *Vision Res.* **7**:253.

BRINDLEY, G. S. 1956. *J. Physiol. (London).* **134**:360.

BROWN, K. T. 1968. *Vision Res.* **8**:633.

BYZOV, A. L. 1965. *Cold Spring Harbor Symp. Quant. Biol.* **30**:547.

CALDWELL, P. C. 1968. *Physiol. Rev.* **48**:1.

CARSLAW, H. S., and J. C. JAEGER. 1959. Conduction of Heat in Solids. The Oxford University Press, London.

COLE, K. S. 1968. Membranes, Ions, and Impulses. University of California Press, Berkeley.

DAVIES, H. G. 1958. *In* General Cytological Methods. J. F. Danielli, editor. Academic Press, Inc., New York. **1**:55.

DERKSEN, H. E., and A. A. VERVEEN. 1966. *Science (Washington).* **151**:1388.

GRANIT, R. 1963. Sensory Mechanisms of the Retina. Hafner Publishing Co., Inc., New York.

GUEST, P. G. 1961. Numerical Methods of Curve Fitting. Cambridge University Press, London.

HAGINS, W. A. 1957. Rhodopsin in a Mammalian Retina. Ph.D. Thesis, Cambridge University, Cambridge.

HAGINS, W. A. 1965. *Cold Spring Harbor Symp. Quant. Biol.* **30**:403.

HECHT, S., S. SHLAER, AND M. H. PIRENNE. 1942. *J. Gen. Physiol.* **25**:819.

JEANS, J. H. 1951. The Mathematical Theory of Electricity and Magnetism. Cambridge University Press, London.

KANEKO, A., and H. HASHIMOTO. 1967. *Vision Res.* **7**:847.

LANING, J. H., AND R. H. BATTIN. 1956. Random Processes in Automatic Control. McGraw-Hill Book Company, New York.

LASANSKY, A., and F. W. DE FISCH. 1966. *J. Gen. Physiol.* **49**:913.

LAWSON, J. L., AND G. E. UHLENBECK. 1950. Threshold Signals. M.I.T. Radiation Laboratory Series. McGraw-Hill Book Company, New York **24**:74.

LIEBMAN, P. A., and G. ENTINE. 1968. *Vision Res.* **8**:761.

NILSSON, S. E. G., and F. CRESCITELLI. 1969. *J. Ultrastruct. Res.* **27**:45.

OVERBEEK, J. TH. G. 1953. *J. Colloid Sci.* **8**:593.

PENN, R. D., and W. A. HAGINS. 1969 *a*. Abstracts of the Biophysical Society 13th Annual Meeting. Biophysical Society, New York. A244.

PENN, R. D., and W. A. HAGINS. 1969 *b*. *Nature (London).* **223**:201.

RICE, S. O. 1954. Mathematical Analysis of Random Noise. *In* Noise and Stochastic Processes. N. Wax, editor. Dover Publications, Inc., New York.

SCHANNE, O. F. 1969. *In* Glass Microelectrodes. M. Lavallée, O. F. Schanne, and N. C. Hébert, editors. John and Sons, Inc., New York. 299–321.

SIDMAN, R. L. 1957. *J. Biophys. Biochem. Cytol.* **3**:15.
SVAETICHIN, G., K. NEGISHI, and R. FATECHAND. 1965. *In* Ciba Foundation Symposium on Color Vision: Physiology and Experimental Psychology. A. V. S. de Reuek and J. Knight, editors. Little, Brown and Company, Boston. 178.
TERMAN, F. E. 1943. Radio Engineer's Handbook. McGraw-Hill Book Company, New York. 173.
TOMITA, T. 1963. *J. Opt. Soc. Amer.* **53**:49.
TOYODA, J., H. NOSAKI, and T. TOMITA. 1969. *Vision Res.* **9**:453.
WACHPRESS, E. L. 1960. *In* Mathematical Methods for Digital Computers. A. Ralston and H S. Wilf, editors. John Wiley and Sons, Inc., New York.
WALLS, G. L. 1942. The Vertebrate Eye and its Adaptive Radiation. Cranbrook Institute of Science, Bloomfield Hills, Mich.
WERBLIN, F. S., and J. E. DOWLING. 1969. *J. Neurophysiol.* **32**:339.
YOUNG, R. W. 1967. *J. Cell Biol.* **33**:61.